

Rain-wind induced vibration of inclined stay cables. Part I: Experimental investigation and physical explanation

Nicola Cosentino[†]

DISTART, University of Bologna, Via Risorgimento 2, 40136 Bologna, Italy

Olivier Flamand[‡]

Centre Scientifique et Technique du Bâtiment, 11 rue Henri Picherit, 44000 Nantes, France

Claudio Ceccoli^{‡†}

DISTART, University of Bologna, Via Risorgimento 2, 40136 Bologna, Italy

(Received September 9, 2002, Accepted November 4, 2003)

Abstract. The rain-wind induced vibration of stays is a phenomenon discovered recently and not well explained yet. As it is influenced by a wide range of physical parameters (cable size and shape, wind speed, direction and turbulence, rain intensity, material repellency and roughness, cable weight, damping and pre-strain), this peculiar phenomenon is difficult to reproduce in laboratory controlled conditions. A successful wind tunnel experimental campaign, in which some basic physical quantities were measured, allowed an extensive analysis as to identify the parameters of the rain-wind induced excitation. The unsteady pressure field and water thickness around a cable model were measured under rainy-excited conditions. The knowledge of those parameters provided helpful information about the air-flow around the cable and allowed to clarify the physical phenomenon which produces the excitation.

Keywords: wind induced vibrations; rain; cable dynamics; water rivulet; bridges; flow regime.

1. Introduction

Strong vibration of inclined stay cables (up to 2 m amplitude) in moderately windy and rainy days was firstly reported by Hikami in 1986 and subsequently (Hikami and Shiraishi 1988) named as Rain-Wind Induced Vibration (RWIV). Several full-scale observations of RWIV have been reported and some stay cable oscillations observed before 1986 have been also ascribed to RWIV.

Based on wind tunnel investigations, different interpretative models have been proposed in literature. Basically, the galloping instability (due to asymmetry of the cable cross section determined by the formation of a water rivulet on the upper part of the cable) and the three-

[†] Research fellow

[‡] Research Engineer

^{‡†} Professor

dimensional effects of Karman vortex (enhanced by the axial flow and by the water rivulet) are among the most quoted models. Unfortunately, none of existing models is able to accurately describe the full scale observed phenomenon and to provide a quantitative estimation of its features (frequency, amplitude, wind speed, etc.).

The literature on the subject points out different aspects which have to be kept in mind in the RWIV wind tunnel simulation. Firstly, the phenomenon initially described by Hikami and Shiraishi (1988) (which is the topic of the present work) occurs only in a narrow range of different parameters (wind speed 5 to 15 m/s; excited modes frequency 0.6 to 3 Hz; cable diameter 100 to 250 mm; inclined stays declining along-wind, the yaw angle being 20° to 45° ; moderate rain; low wind turbulence).

The rain is an essential parameter and the importance of the surface wet-ability and the upper water rivulet mobility has been pointed out by Flamand (1995). The water pulverization system has to be carefully designed to reproduce the actual rain conditions. Finally, different responses can occur by changing the direction of cable-model mobility (Honda, *et al.* 1995). Thus, the model restraining has to carefully reproduce the actual cable DOFs.

It seems important to observe that the wind excitation of stays in dry conditions (Matsumoto 2000) is characterized by different features (smaller amplitudes, higher frequency, etc.) and is probably determined by different physical phenomena. Following the same point of view, the rain-wind induced vibration of quasi-vertical hangers (Verwiebe and Ruscheweyh 1998, Zasso, *et al.* 1992) could be related to the same physical data as the vibration of declining stays studied in this paper, but the mechanism, the geometric configuration and finally the phenomenon characteristics are rather different and induce the water rivulet(s) to play a different role.

The unsteady pressure fields and water thickness have been firstly measured in the Jules Verne Climatic Wind Tunnel of CSTB under actual, even if artificial, rain. Preliminary results were reported by Flamand, *et al.* (2001). In the present work, an extensive analysis and the interpretation of experimental data (including the re-interpretation of old data) are presented.

2. Experimental setup

The cable model tested at CSTB is made by an iron tube 5.60 m long which is covered by a high

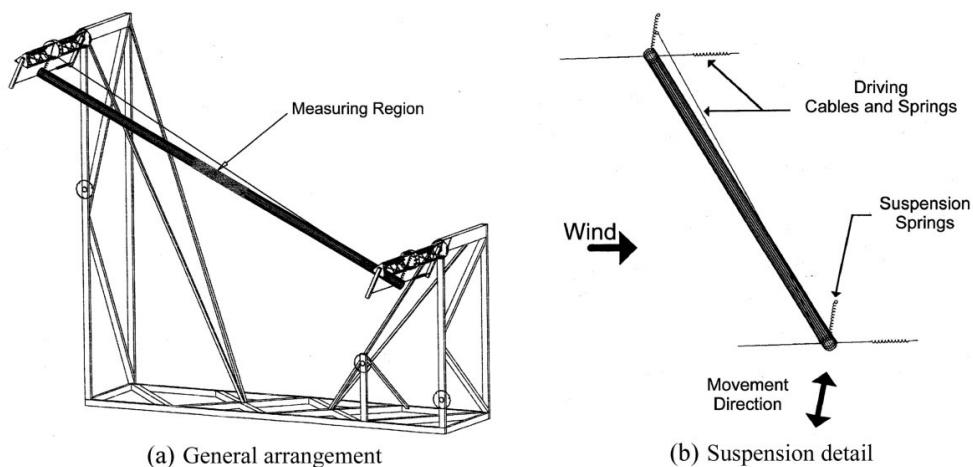


Fig. 1 Model rig: (a) general arrangement and (b) suspension detail

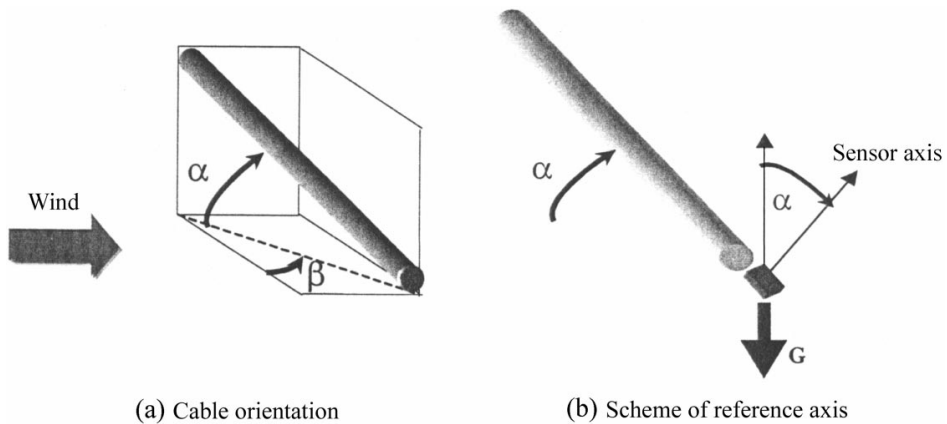


Fig. 2 (a) Cable orientation and (b) scheme of reference axis

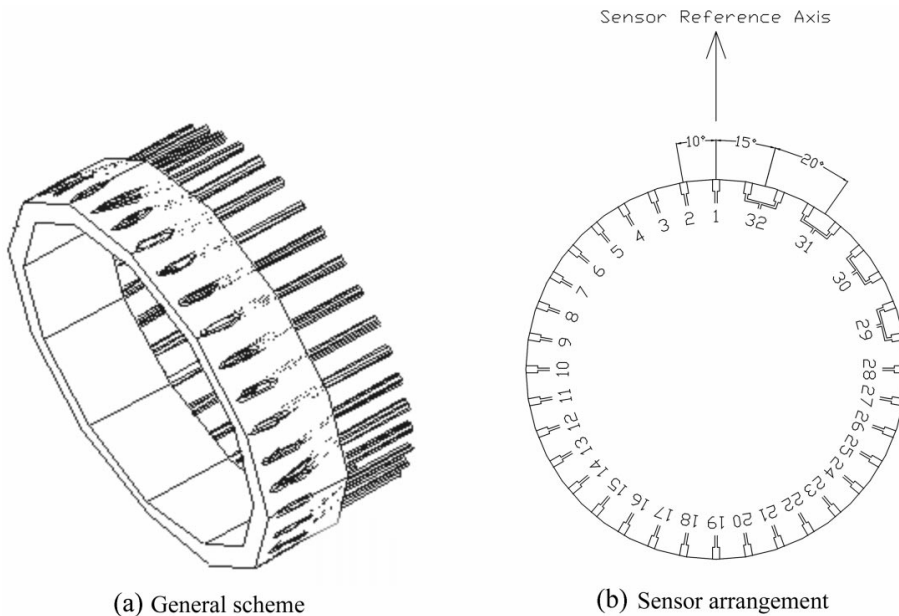


Fig. 3 Water-repellent pressure taps: (a) general scheme and (b) sensor arrangement

density polyethylene (HDPE) sheath of 160 mm external diameter, representing a common solution for existing stays. In order to reproduce the field conditions, the model is suspended by a system of springs and thin cables (Fig. 1(a),(b)) which allows only the movement perpendicular to cable axis, in the vertical plane. In fact, even if the actual cables can move out of plane, the RWIVs usually occurs as in-plane oscillations. The model system is characterised by a main oscillation frequency $f_1=1.08$ Hz. The relative damping for the first mode varies from $\xi=0.08\%$ (for low oscillation amplitudes) to $\xi=0.25\%$ (for higher amplitudes, up to ± 150 mm). The cable inclination (α) and yaw (β) angles can be varied to test different geometrical conditions. Geometrical references are shown in Fig. 2(a),(b).

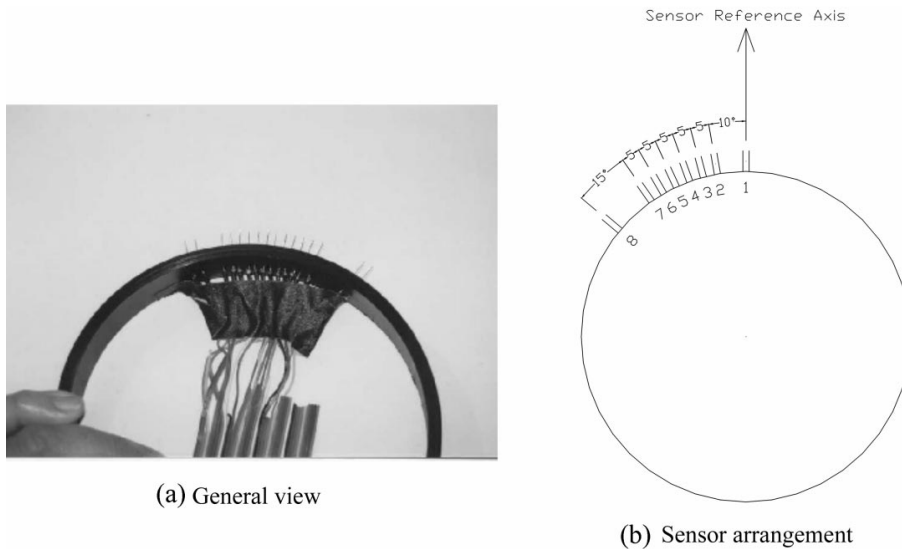


Fig. 4 Water thickness sensor crown (a) general view and (b) sensor arrangement

Due to the impossibility to measure pressures in rainy conditions with classical sensors, the central part of the cable model is equipped by a 36 water-repellent pressure taps crown, specially designed for these tests. It is based on large diameter (3 mm) pressure taps as shown in Fig. 3(a). Each pressure tap is inclined 30° to the cable wall and its inner is covered by silicon oil. Cable inclination to the wind and orifice dimension should avoid the taps filling. Fig. 3(b) shows the sensor arrangement and their numeration with respect to the reference axis. Because the available pressure sensor system had only 32 input channels, the taps 29 to 36 were paired and connected to channels 29 to 32; thus, the instantaneous mean pressure of each pair was measured.

The water thickness is measured by means of paired wires arranged on a HDPE crown as shown in Fig. 4(a). Since the formation and the movement of the upper water rivulet has been recognized to be the main responsible of RWIVs, the instrumented portion of the HDPE crown covers all the cable region where such a rivulet has been observed to take place. Fig. 4(b) shows the sensor arrangement and their numeration with respect to the reference axis. An AC tension difference is applied between the two wires of each couple. The measured current intensity is function of the water thickness. The validation and the calibration of both the pressure and the water sensors are discussed by Flamand, *et al.* (2001) and Cosentino (2002).

The model is also equipped by two accelerometers placed inside the iron tube at its top and at its bottom. Finally, a peacock-tail device is used to spurt an artificial drizzle (similar to the actual RWIV occurrence condition) upstream the model.

3. Experimental results

The rain-wind induced vibration of stay cables has been carefully reproduced by mean of the experimental apparatus above described. The reproduced phenomenon features are in very good agreement with the full scale observations reported by different authors (Hikami and Shiraishi 1988, Main and Jones 1999, Main, *et al.* 2001, Matsumoto, *et al.* 1989).

In order to investigate the influence of different parameters, numerous tests have been carried out in different external conditions. Rain features and cable inclination have shown to be among the governing parameters. In particular, during the tests, the excitation has been observed only in presence of moderate artificial rain. Too light or strong rainfall give rise to none or small vibrations even when the other parameters are favourable to the excitation. It is important to observe that excitation has never been observed without the formation of the upper rivulet. Different materials have been used for the external sheath: in all cases the rivulet can be easily formed if the surface is dirty, as it is usually on existing cables, due to the atmospheric pollution. The rainfall and the covering material influence the washability of the cable surface and, thus, the rivulet formation (Flamand 1995).

No excitation has been observed for horizontal cable model ($\alpha=0$) in both rainy and dry conditions. In addition, the yaw angle range that gives rise to excitation is the same as reported in literature and shown in Fig. 5(a). Largest vibrations have been observed at about $\beta=20^\circ\div30^\circ$. Values of β greater than 60° or negative, are unfavorable to the excitation. The limited wind speed range characteristic of rain-wind induced vibration is clearly highlighted by experiments, being 7 to 12 m/s the worst conditions for the given cable properties (Fig. 5(b)). Furthermore, the exciting wind speed increases as the yaw angle increases (Fig. 5(b)), so that the normal to the cable wind speed seems to be a better representative parameter (see also Fig. 5(c)).

It is also important to observe that RWIV occurs within a limited range of Reynolds number which corresponds to the upper sub-critical one. This circumstance is pointed out by different full-

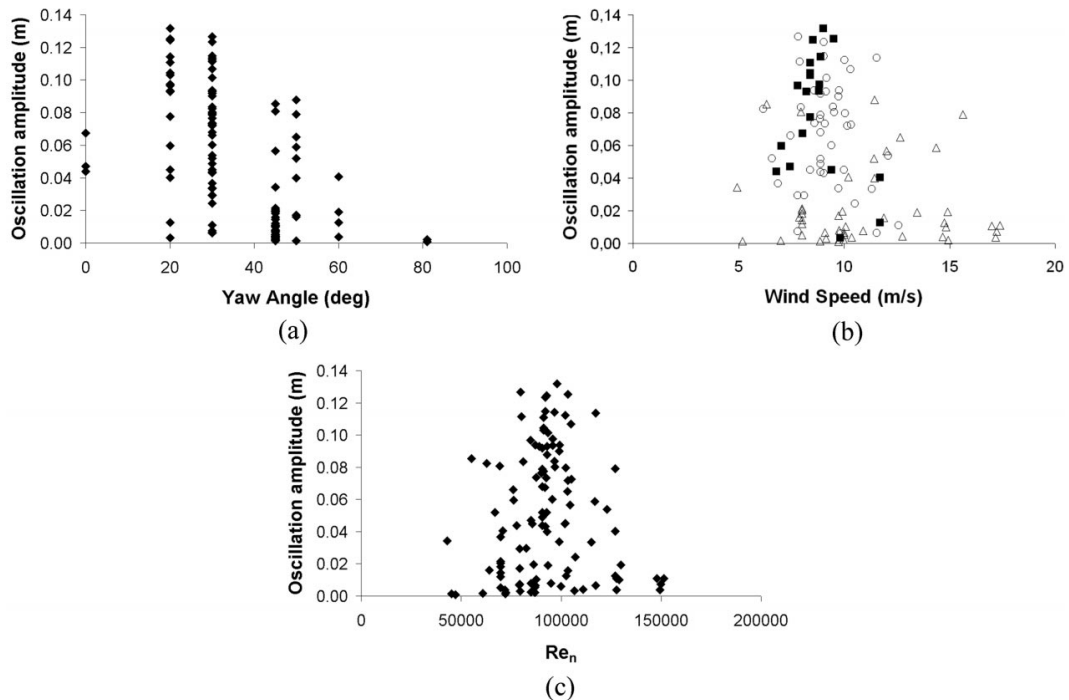


Fig. 5 Influence of (a) the yaw angle, (b) the absolute wind speed - squares: $\beta=0^\circ\div20^\circ$; circles: $\beta=30^\circ$; triangles: $\beta=45^\circ\div80^\circ$ - and (c) the Reynolds number on the cable model induced oscillations measured in wind tunnel

scale observations (Matsumoto, *et al.* 1989, Larose and Zan 2001) even if it has not been taken into account in the interpretative models proposed in literature. The present wind tunnel tests confirm this feature as shown in Fig. 5(c), where the Reynolds number is referred to the normal to the cable wind speed:

$$Re_n = \frac{V \cos \beta^* D}{\nu} \quad (1)$$

β^* being the effective yaw angle, V the undisturbed mean wind speed, ν the kinematic viscosity.

3.1. Pressure fields

The measurements of pressure fields around the cable have been carried out under a wide range of external conditions able to excite the cable and also in absence of excitation and/or in absence of rain.

Firstly, a roughness effect induced by rain is pointed out by the mean pressure distribution. In fact, a given set of external parameters which, in dry conditions, produces a typical sub-critical pressure distribution, in presence of rain, it is characterised by a critical pressure distribution (that is, a sudden decrease of negative pressure leeward their maximum value and a large base-pressure region). Fig. 6(a),(b),(c) show this effect by mean of two tests carried out at $V=12$ m/s, $\alpha=25^\circ$,

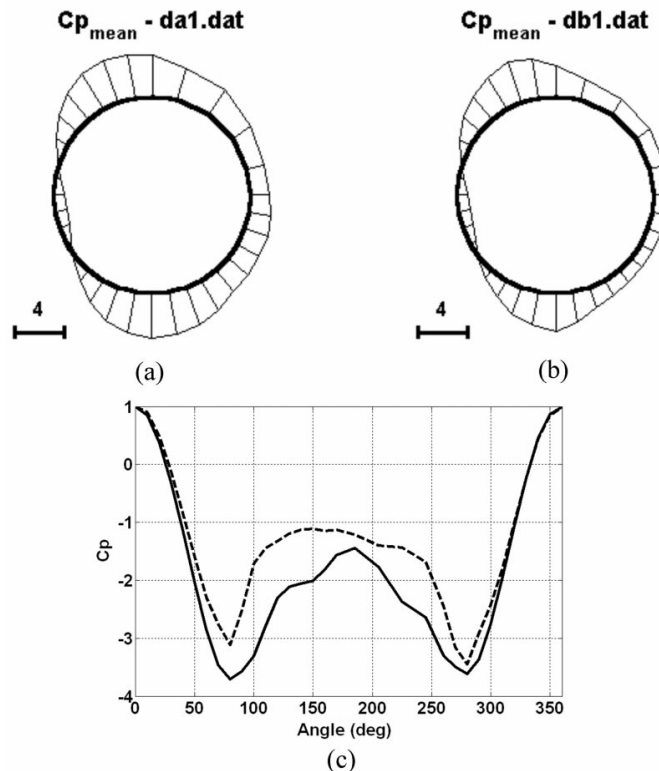


Fig. 6 Pressure distribution in (a) dry and (b) rainy conditions; (c) comparison in Cartesian diagram: solid = dry, dashed = rainy - angles anticlockwise from the stagnation point

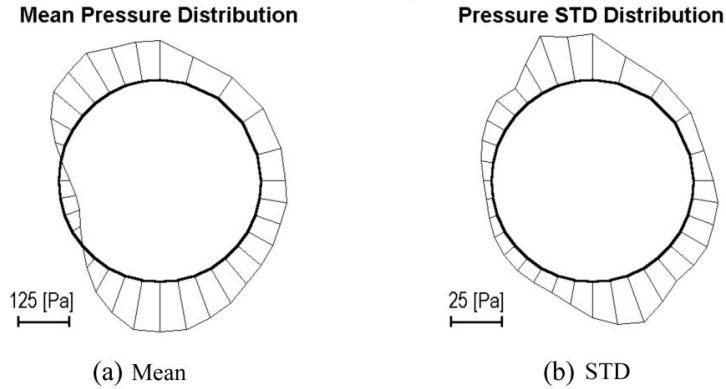


Fig. 7 Main pressure statistics in excited conditions ($U=9$ m/s, $\alpha=25^\circ$, $\beta=30^\circ$): (a) mean, (b) STD

$\beta=30^\circ$, without rain (*dal.dat* – no excitation) and with rain (*dbl.dat* – before the excitation took place) respectively. As a matter of fact, even if RWIVs usually occurs at $Re \cong 1 \times 10^5$, due to the water roughness effect, this value of Re “falls” in the critical range.

Fig. 7 shows the main statistic properties of pressure field in rainy and exciting conditions. The deviation of the stagnation point with respect to the horizontal direction is determined by the yaw and inclination angles following the well known law:

$$\gamma = 90^\circ - \arccos\left(\frac{\sin \alpha \sin \beta}{\sqrt{\sin^2 \alpha + \cos^2 \alpha \cos^2 \beta}}\right) \quad (2)$$

In particular, Fig. 7(a) shows the mean pressure distribution; it can be observed a non-symmetry in mean pressures determined by the exciting mechanism, as it will be explained below. The unsteady pressures and the resultant lift force are characterized by a main frequency content which coincides with the cable frequency, independently from the wind speed (Fig. 8(a),(b),(c)). Moreover, the classical Karman vortices, usually pointed out by the presence of an important content at the Strouhal frequency in the PSDF, disappear (become very broad-band) for yaw angles $\beta^* > 25^\circ \div 30^\circ$, as besides reported by Bursnall and Loftin (1951).

The aerodynamic power has been evaluated by correlating the unsteady pressures and the cable motion. In Fig. 9(a), the unsteady lift force, the instantaneous power and the cumulative work are shown. It can be observed that the aerodynamic power is made by a series of positive and negative peaks, the positive ones being dominant. Furthermore, the statistic distribution of the lift force is characterised by the dominant presence of negative peaks as shown in Fig. 9(b). It is also interesting to observe (the physical explanation will be given below) that the positive work is furnished to cable in the cross-wind directions, independently from the cable movement direction (Fig. 9(c)). In fact, the presence of two “positive power lobes” at $\pm 90^\circ$ from the stagnation point is confirmed by different γ values even if the cable movement is always in the vertical plane.

In order to outline the stochastic regularity (during numerous cable cycles) of the measured quantities without losing information about sudden peaks, the given quantity has been monitored for different cable cycles in dynamically steady state. It has been superposed for all the cycles of a

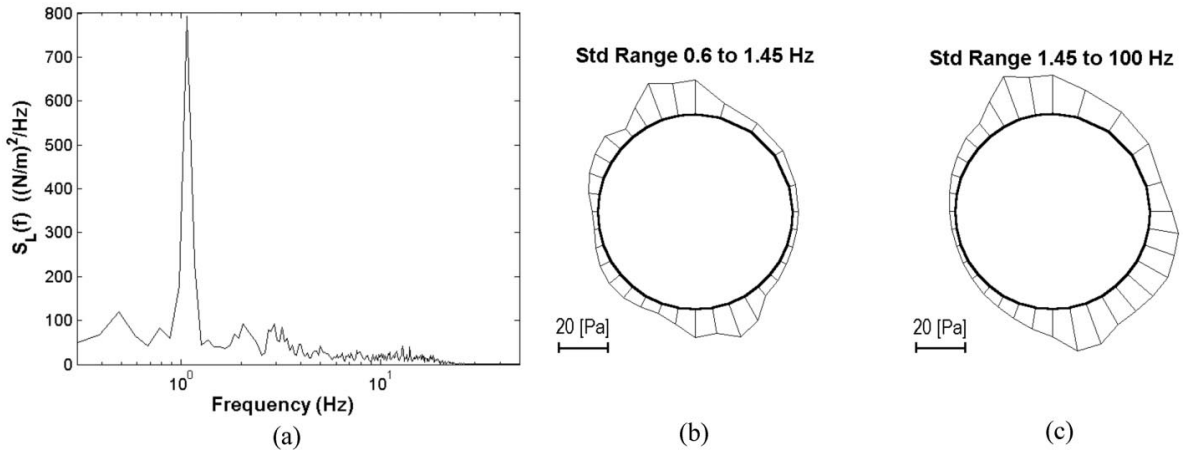


Fig. 8 (a) PSDF of lift force and (b),(c) distribution of frequency contributions in terms of STD ($U=9$ m/s, $\alpha=25^\circ$, $\beta=30^\circ$)

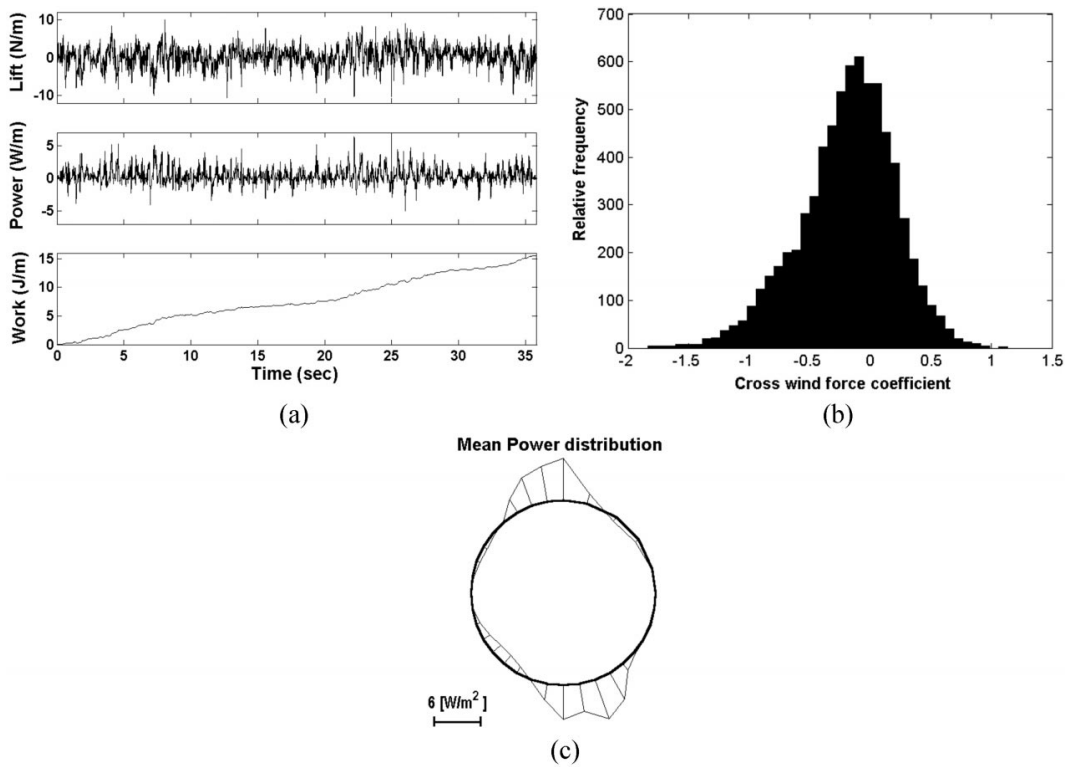


Fig. 9 (a) Time history traces of lift force, power and cumulative work, (b) histogram of cross wind force coefficient and (c) mean aerodynamic power distribution around the cable

given recorded time history (40 or more) and a sort of “mean cycle” has been derived. At each cable position within the “mean cycle”, corresponds a statistic distribution of the monitored quantity. Fig. 10 shows, for instance, the mean value of such distribution along the “mean cycle”,

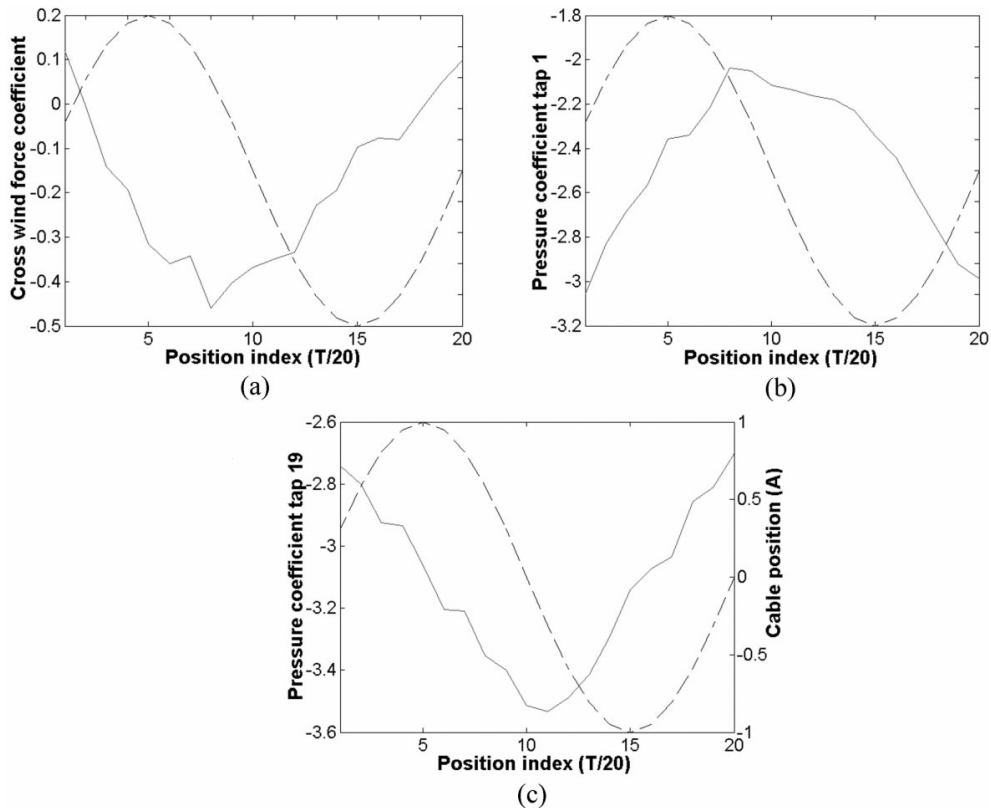


Fig. 10 Mean cycle evolution of (a) cross wind force coefficient, (b) pressure coefficient at the cable top and at (c) the cable bottom. Dashed lines represent the normalized cable position

relative to the cross wind force coefficient (Fig. 10(a)), the pressure coefficient close to the upper separation point (tap 1 - Fig. 10(b)) and the lower one (tap 19 - Fig. 10(c)), respectively.

For pressures and forces, the mean cycle well represents the aerodynamic power generation mechanism. Fig. 10(a) points out that the aerodynamic power is produced by a downward crosswind force occurring (preferentially: the mean cycle analysis points out the tendency of a stochastic process) during the descending motion of the cable. In particular, such a cross-wind force is determined by a decrease of the upper negative pressures (Fig. 10(b)) followed, within a short time lag compared to the cable cycle, by an increase of lower negative pressures (Fig. 10(c)). As a matter of fact, the analysis of the complete statistic distribution at different points of the mean cycle (histograms - here omitted for space reasons - whose mean values are given in Fig. 10) shows that the negative peaks in the cross wind force (Fig. 9(b)) occur preferentially during the descending cable motion giving rise to an averaged downward force (Fig. 10(a)) and a subsequent positive aerodynamic power.

3.2. Water movements

The time history traces of the water thickness show that the upper rivulet is composed by a “base carpet” and an oscillating “wave” which slides on the former. This is clear from Fig. 11(a) where a

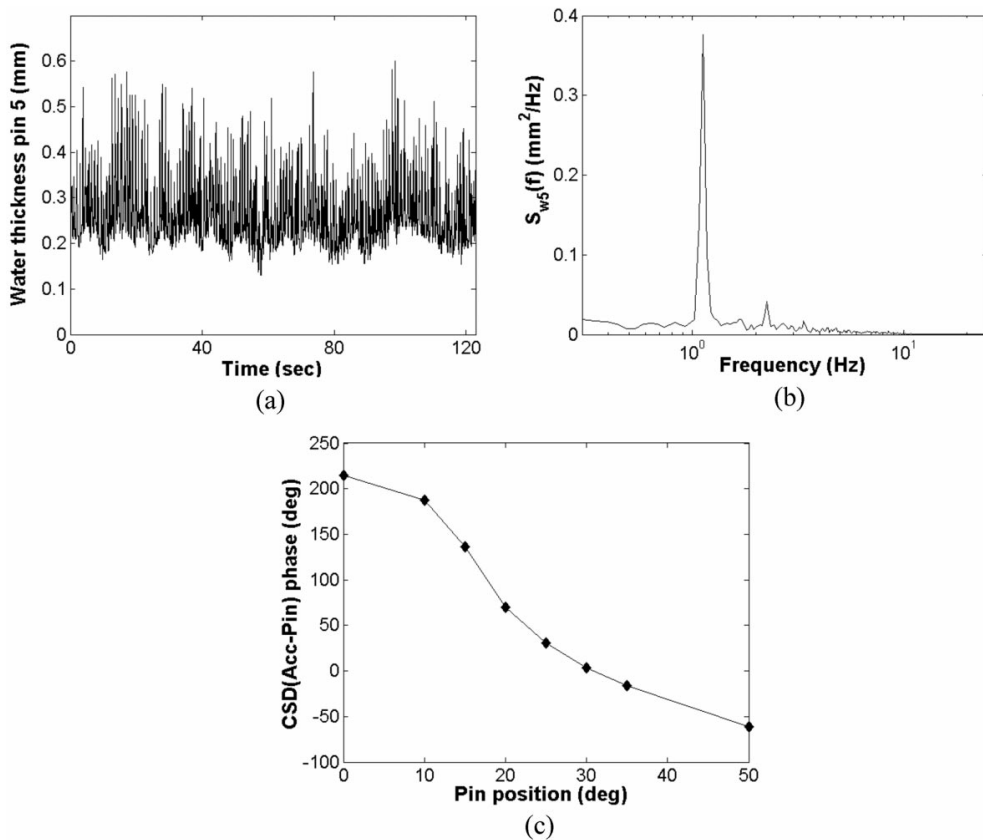


Fig. 11 (a) Typical time history record of a water thickness measurement, (b) its PSDF and (c) phase lag between cable acceleration and water thickness measurements

typical time history trace recorded at the water thickness sensors is shown. In the following analysis, the attention is focused on the fluctuating wave, simply named as rivulet. The water thickness measurements allow to determine the rivulet instantaneous position (barycentre) and dimensions referred to the instantaneous shape measured by the eight pins (without taking into account the uniform and constant base carpet). As a matter of fact, the only order of magnitude of the rivulet dimensions is reliable; in fact, the surface tension effects, between water and metallic pins, can smooth the water thickness peaks.

The frequency content of both rivulet position and single pin measurements coincide substantially with the cable frequency (Fig. 11(b)), independently from the other external conditions as, for instance, the wind speed. It means that: (1) the rivulet is not characterized by a natural frequency (at the contrary of what is hypothesized by Yamaguchi 1990) and (2) the rivulet crosses each sensor once per cable cycle and not twice (as it is expected). As a matter of fact, a careful analysis shows that the rivulet is well marked during its descending (windward, i.e., from pin n. 1 towards pin n. 8 as in Fig. 4(a)) motion; it spreads when it reaches the lowest position and it slides back (leeward, i.e., from pin n. 8 towards pin n. 1) in a disorganized way, probably through the base carpet. This hypothesis is confirmed by the phase lag evolution between the water thickness records and the

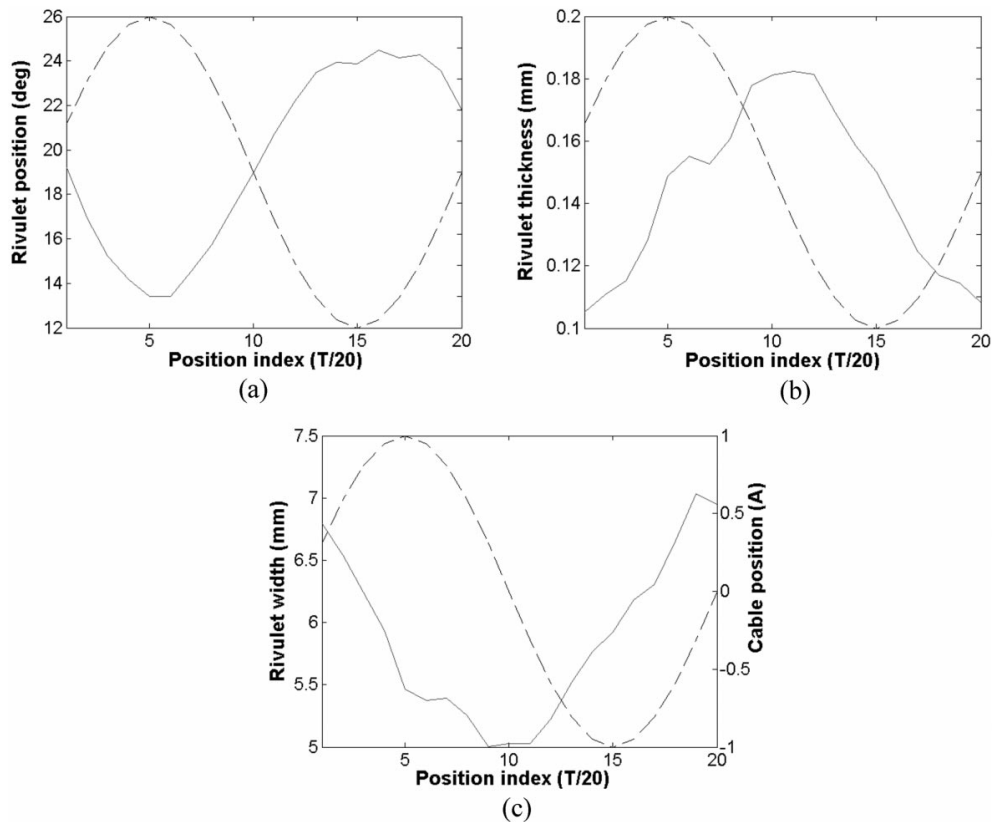


Fig. 12 Mean cycle evolution of (a) rivulet position, (b) thickness and (c) width. Dashed lines represent the normalized cable position

cable acceleration (Fig. 11(c)) and, even more clearly, by the “mean-cycle” behaviour of rivulet position, thickness and width (Fig. 12(a),(b),(c)). In Figs. 11(c) and 12(a), pin and rivulet positions are measured anticlockwise to the vertical direction (according to Fig. 4(b)).

The rivulet movement features above described are also confirmed by the observation of video movies which have been recorded during experiments in exciting conditions.

4. The RWIV mechanism

Taking into account the rain induced “roughness effect”, the RWIVs occur between the critical and the sub-critical Re range. Literature on flow around circular cylinders (Thompson 1980, Zdravkovich 1997), reports the occurrence of very complex aerodynamic phenomena within this range. In particular, it is pointed out that the well known drag-crisis is determined by the reattachment of the separated laminar boundary layer (and a subsequent decrease of negative pressures) before the definitive turbulent separation in the wake (bubbles regimes - Fig. 13). The phenomenon is stochastically symmetric but, in presence of obstacles close to the separation point, it will preferably occur at the obstacle location side (one bubble regime), giving rise to a mean cross-wind force which can reach the same order of magnitude as the drag force.

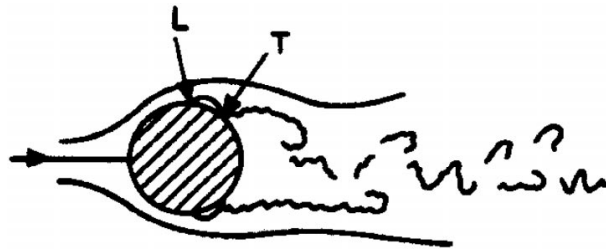


Fig. 13 The “bubble regime”. L =laminar boundary layer separation; T =turbulent boundary layer separation after reattachment

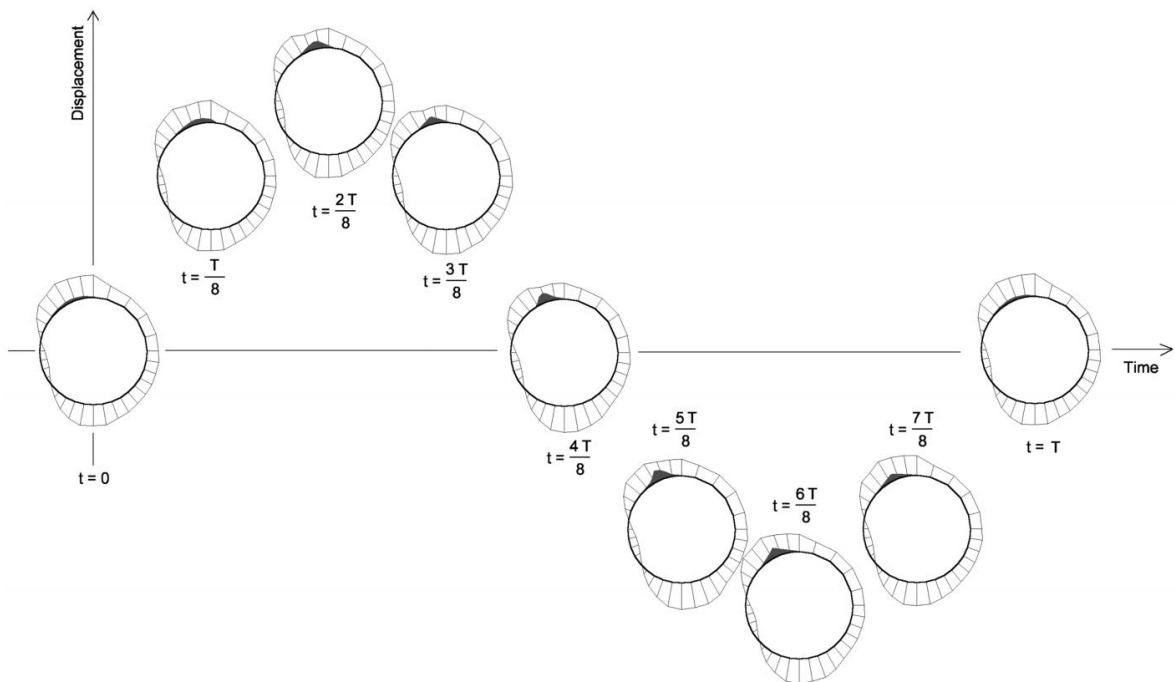


Fig. 14 Superposed mean cycle evolution of pressure distribution and water thickness

Fig. 14 resumes the experimental “mean cycle” evolution of pressure field and water thickness in excited conditions. The water thickness scale has been enlarged for a better representation while, due to the small scale, the rivulet circumferential oscillations can be better seen in Fig. 12(a). The pressure behaviour and the subsequent exciting mechanism can be explained by the light of the above cited critical flow regime properties (the process, of course, is stochastic and the interpretation has to be meant in the “mean cycle” sense).

As the cable goes up and its acceleration becomes negative, due to the inertial effects, the originally spread rivulet gathers at the top of the cable ($t=T/8$ to $2T/8$). The rivulet thickness increases and, thus, an obstacle is formed close to the upper boundary layer separation point ($\cong 90^\circ$ from the incidence direction). The one-bubble regime is developed and it is pointed out by the negative upper pressure reduction. This regime persists during all the descending cable

movement ($t=2T/8$ to $5T/8$). Meanwhile, the decrease of upper negative pressures produces an overpressure in the wake which, in turn, pushes down the lower flow and produces the lower negative pressure increase above cited (Fig. 10(b),(c)). Then, due to the variations in the cable acceleration and the subsequent inertial effects, the rivulet is pushed down descending (windward, i.e. from pin n. 1 towards pin n. 8 as in Fig. 4(a)) and it goes away from the separation point. In addition, it becomes spread and irregular ($t=5T/8$ to $7T/8$). Thus, the obstacle effect is reduced and the upper reattachment occurrence probability decreases. The inversion of the cable acceleration allows the rivulet to slide up (leeward, i.e. from pin n. 8 towards pin n. 1) even if in a disorganized way and through the base carpet ($t=7T/8$ to $T/8$). The process starts again. As a matter of fact, the bubble regime disappears for yawed cylinders if the effective yaw angle β^* is larger than $30^\circ \div 40^\circ$ (Bursnall and Loftin 1951) and this explains the restricted yaw angle range which gives rise to RWIVs.

It seems important to underline that the pressure fluctuations are sudden, sharp and random in occurrence and intensity. The mean cycle representation certainly smoothes the pressure peaks but it well points out the base regularity, which is responsible for the exciting process.

Furthermore, the flow regime is influenced, not only by the rivulet, but also by the relative angle of attack; in fact, the water carpet must be close to the separation point to determine the one-bubble regime. The angle of attack is determined by the rivulet movement and, as the cable excitation takes place and the oscillation amplitude increases, by the cable movement itself. These aspects have to be taken into account in numerically modelling the phenomenon; they also have to be studied deeper by further specific wind tunnel tests.

Finally, it is opportune to highlight that the present research has been limited to the RWIVs of inclined stays ($20^\circ < \alpha < 50^\circ$, as order of magnitude). The rain-wind induced vibration of quasi-vertical hangers (Verwiebe and Ruscheweyh 1998, Zasso, *et al.* 1992) have not been treated in this paper. In such cases, the presence of a lower rivulet plays an important role. Maybe, the exciting mechanism (that is, the periodic presence of the one bubble regime) could be the same in inclined and quasi-vertical cables; probably it is a different one, related to the shape modification due to the presence of large water rivulet, close to the galloping of bundle iced conductors. This has to be proved or refuted by measuring the unsteady pressures around quasi vertical hangers also. Specific tests will be necessary to compare the RWIV mechanism on inclined and on quasi-vertical cables.

5. Conclusions

The rain-wind induced vibration of stay cables have been successfully reproduced by climatic wind tunnel tests. Furthermore, the unsteady pressures and water thickness have been measured – for the first time, in authors knowledge – in actual, even if artificial, rainy conditions. The knowledge of these quantities allowed an original interpretation of the exciting mechanism. In fact, the RWIV is determined by a flow regime modification which occurs close to the critical Re range. Such flow regime fluctuations are related to the air-rivulet interference. They are quite random but, due to the cable-rivulet movement synchronisation, they are characterised by a certain regularity which gives rise to a cumulative positive aerodynamic work and, subsequently, to the excitation.

Further wind tunnel tests will be necessary to accurately quantify the air-rivulet interference parameters and rivulet hydro-dynamics.

References

- Burnsall, W.J. and Loftin, L.K. (1951), "Experimental investigation of the pressure distribution about a yawed circular cylinder in the critical Reynolds number range", NACA TN 2463, Washington.
- Cosentino, N. (2002), "Rain-wind induced vibrations of stay cables", Ph.D. Thesis, University of Bologna, Bologna.
- Flamand, O. (1995), "Rain-wind induced vibration of cables", *J. Wind Eng. Ind. Aerodyn.*, **57**, 353-362.
- Flamand, O., Peube, J.L. and Papanikolas, P. (2001), "An explanation of the rain-wind induced vibration of inclined stays", *Proceedings of 4th International Symposium on Cable Dynamics*, Montréal, May.
- Hikami, Y. and Shiraishi, N. (1988), "Rain-wind induced vibrations of cables in cable stayed bridges", *J. Wind Eng. Ind. Aerodyn.*, **29**, 409-418.
- Honda, A., Yamanaka, T., Fujiwara, T. and Saito, T. (1995), "Wind tunnel test on rain-induced vibration of the stay-cable", *Proceedings of International Symposium on Cable Dynamics*, Liege.
- Larose, G.L. and Zan, S.J. (2001), "The aerodynamic forces on the stay cables of cable-stayed bridges in the critical Reynolds number range", *Proceedings of 4th International Symposium on Cable Dynamics*, Montréal, May.
- Main, J.A. and Jones, N.P. (1999), "Full scale measurement of stay cable vibration", *Proceedings of Wind Engineering into the 21st Century*, Rotterdam.
- Main, J.A., Jones, N.P. and Yamaguchi, H. (2001), "Characterisation of rain-wind induced stay-cable vibrations from full-scale measurements", *Proceedings of 4th International Symposium on Cable Dynamics*, Montréal, May.
- Matsumoto, M. (2000), "Vortex-excited vibration and galloping instability of inclined cables", *Proceedings of 6th Italian Conference on Wind Engineering, IN-VENTO-2000*, Genova, June.
- Matsumoto, M., Yokohama, K., Miyata, T., Fujino, Y. and Yamaguchi, H. (1989), "Wind-induced cable vibration of cable-stayed bridges in Japan", *Proceedings of Japan Canada joint Workshop on Bridge Aerodynamic*, Japan.
- Thompson, N. (1980), *Mean Forces, Pressures and Flow Field Velocities for Circular Cylindrical Structures: Single Cylinder with Two-Dimensional Flow*, ESDU Data Item 80025, London.
- Verwiebe, C. and Ruscheweyh, H. (1998), "Recent research results concerning the exciting mechanisms of rain-wind-induced vibration", *J. Wind Eng. Ind. Aerodyn.*, **74-76**, 1005-1013.
- Yamaguchi, H. (1990), "Analytical study on growth mechanism of rain vibration of cables", *J. Wind Eng. Ind. Aerodyn.*, **33**, 73-80.
- Zasso, A., Boccione, M. and Brownjohn, J. (1992), "Rain-wind aeroelastic instability of the inclined hangers of a suspension bridge", *Proceedings of Inaugural Conference of the Wind Engineering Society*, Cambridge, September.
- Zdravkovich, M.M. (1997), *Flow Around Circular Cylinders*, Oxford University Press, Oxford.